

A Deep Learning Method for Diagnosing Coronary Artery Disease using SPECT Images of Heart

Nguyen Thanh Trung^{1*}, Nguyen Thai Ha², Nguyen Duc Thuan², Dang Hoang Minh³

¹108 Military Central Hospital, No. 1, Tran Hung Dao, Hai Ba Trung, Ha Noi, Viet Nam

²Hanoi University of Science and Technology, No. 1, Dai Co Viet, Hai Ba Trung, Ha Noi, Viet Nam

³Military Information Technology Institute, No. 17 Hoang Sam, Cau Giay, Ha Noi, Viet Nam

Received: November 01, 2019; Accepted: June 22, 2020

Abstract

Coronary artery disease (CAD) is one of the leading causes of death in the world, especially in the middle-aged and old populations. CAD treatment costs are very high when patients are at a late stage, complicated pathologies. This study investigated the efficiency of the diagnoses of CAD by a deep learning model using polar maps and slice images derived from myocardial perfusion imaging (MPI) by single photon emission computed tomography (SPECT) cameras. Data for evaluation were collected at the Department of Nuclear Medicine, 108 Military Central Hospital. The experimental results showed that learning from MPI slice images provided a higher diagnosis accuracy than from polar map images.

Keywords: SPECT, deep learning (DL), coronary artery disease (CAD), Myocardial Perfusion Imaging (MPI)

1. Introduction

Coronary artery disease (CAD) is a modern-world medical issue of interest because of its rising incidence and the leading cause of death and disablement. The medical fee for the treatment of CAD is high, especially when the patient is in the late stage or has complications [1]. The detection of CAD is based on myocardial perfusion imaging (MPI) by using SPECT camera. In the United States, there are about 7 million SPECT scanning sessions every year [2]. If the CAD is detected in the early stage, the patient can be effectively cured and has a high chance of survival. However, the accuracy of the doctor's decision depends on many factors, including image quality and the doctor's expertise. Applying machine learning for CAD diagnosis is one of the solutions that help to improve the accuracy of the detection.

Machine learning for medical diagnosis has been approached for a long time [3]. Currently, deep learning (DL) which is a broader family of machine learning provides many impressive results for the medical diagnosis problem [4-6]. CAD diagnosis using DL based polar map on stress MPI with total perfusion deficit was introduced in [7]. In the existing work, the DL model is constructed of convolutional neural networks (CNN) layers and three fully connected (FC) layers. The output of the DL model is the weight (ranging 0-1), in which a patient is decided to have CAD if the output weight is greater than 0.7 and not have CAD if the weight is 0.7 or smaller. The

DL model was trained on a dataset of 1,638 polar images (1,018 images of CAD and 620 images of non-CAD). The precision of the DL model is 82.3%.

Polar images are synthesized from slice images by an algorithm which is based on the standardized myocardial segmentation and nomenclature for tomographic imaging of the heart [8,9]. This is suggested by the American Society of Nuclear Cardiology (ASNC). There may have some disease features that are missed in the synthetic procedure. In this study, we consider using the SPECT images for diagnosing CAD because the polar map is derived from these images and may not maintain as many features as the original images. We also introduce a deep learning model to diagnose the CAD from SPECT images.

2. Dataset and diagnosis model

2.1 Dataset

Zeiler and Fergus demonstrate that a CNN layer can learn the features, such as color and edge, which form the object in the input image [10]. Therefore, we used CNN layers to learn the characteristic medical signs of disease in SPECT images. However, to obtain the best benefit of the CNN layer, a large dataset is necessary.

2.1.1. Spect dataset

The dataset was collected at the Department of Nuclear Medicine, 108 Military Central Hospital. It

* Corresponding author: Tel.: (+84) 988.335.388
Email: trung.ntncs16082@sis.hust.edu.vn

includes 1413 heart SPECT images which were scanned from 2015 to 2018. SPECT images were labeled as CAD and non-CAD by many experts. The detail of the dataset is shown in Table 1. The dataset was approved by the ethics committee of the Department of Nuclear Medicine, 108 Military Central Hospital, and it has been used as a reference dataset for the CAD diagnosis.

Table 1: SPECT dataset.

| | CAD | Non-CAD |
|--------------|------------|------------|
| Male | 638 | 477 |
| Female | 134 | 164 |
| Total | 772 | 641 |

In this study, we used polar map on stress MPI and slice MPI to detect the CAD. The other patient's information, such as age, the number of injured coronary artery branches, the test result before MPI scanning, is not of our interest.

2.1.2. Data acquisition

Data were collected from rest and stress MPI sessions which are based on the Bruce protocol about imaging guidelines for nuclear cardiology of the ASNC. Before scanning 60 minutes, the patient was injected with 0,31mCi/kg of radioactive tracer Tc^{99m} -MIBI for each rest and stress phases. For patients who cannot exercise, Dipyridamole was used with 0,56mg/kg/ 4 minutes after heart frequency getting 85% of theory [11,12]. Fig.1 shows the procedure of the two-phase MPI.

The SPECT cameras are Optima 640, Infinia and Ventri, from GE Healthcare. The imaging procedure and parameters are set as default as GE's guidelines. The image quality is verified by doctors with using of specified softwares, such as QGS/QPS, in the Xeleris servers.

Slice images were reconstructed by the iterative optimization algorithm from SPECT cameras. Noise can be removed by imaging when the patient was prone or by the attenuation correction.

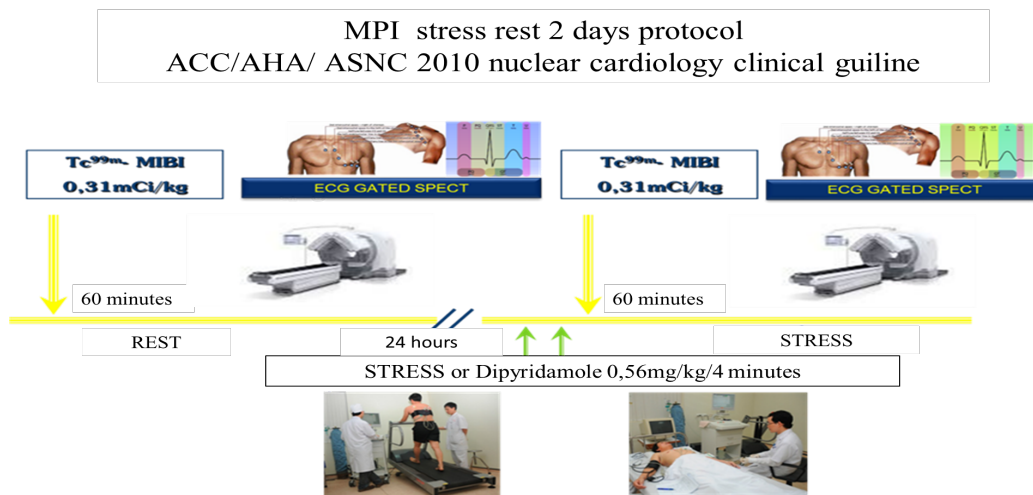


Fig. 1. Procedure of the two-phase myocardial perfusion imaging.

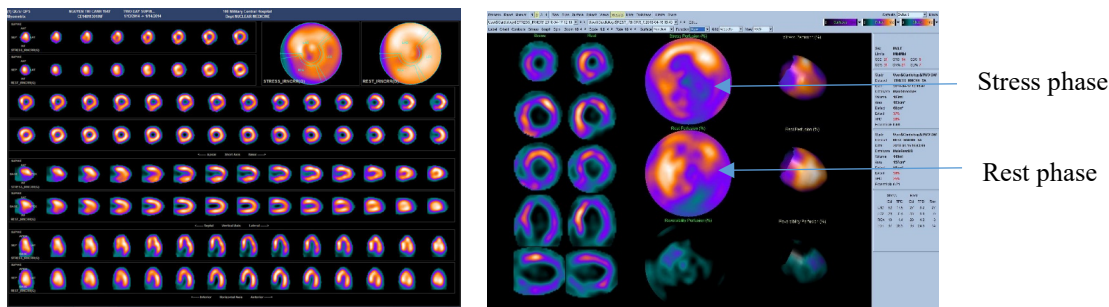


Fig. 2. An example of slice images (left) and polar images (right). The left picture contains 8 rows of images, grouped as 4 pairs of stress (above) and rest (below) phases. From top-to-bottom, pairs are images of two short axes, a vertical long axis, and a horizontal long axis. The right images are polar images which are derived from slice images.

2.1.3. Image preprocessing

The image processing scheme is shown in Fig.3. First, the boundaries around the left ventricular myocardium are provided by the Myovation Evolution tool in Xeleris software, supported by GE Healthcare [13]. The boundaries are adjusted and verified by technicians with more than 15 years of experiences. Doctors double-check the region of interest, i.e. left ventricle and valve plane position if necessary. After that, we obtain the slice and polar images.

In a heart SPECT session, we obtain slice images and polar images (see Fig.2). The polar images are derived from slice images by using the standardized myocardial segmentation and nomenclature for tomographic imaging [8,9]. Images were acquired both in rest and stress phases. These images, which represent the anatomical information of the patient’s heart, are then used to diagnose the CAD.

2.1.4. Image normalization

The original size of polar and slice images is $1920 \times 1080 \times 3$ (3 indicates three color channels). Images were cropped by a fixed margin to remove unnecessary information and to reduce the

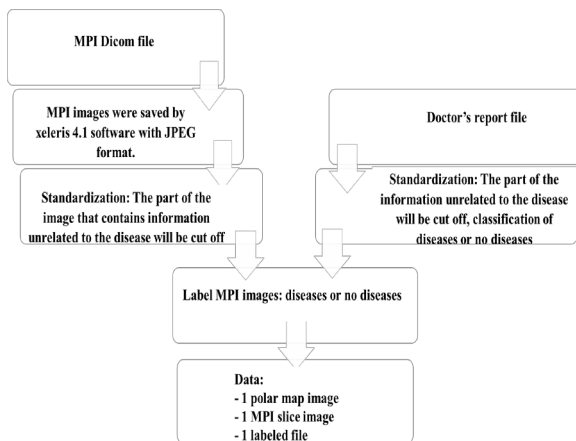


Fig. 3. The image processing scheme of SPECT images.

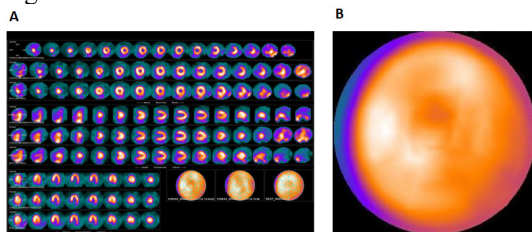


Fig. 4. Cropped slice (A) and polar (B) images of Fig. 2.

computation. Cropped size is $1080 \times 1640 \times 3$ for slice images and $314 \times 314 \times 3$ for polar map image (see Fig.4).

2.1.5. Data labeling

SPECT images of each patient were labeled as CAD or non-CAD. This was done by experts and verified by many-year experient doctors. In case of CAD, doctors specify the injured location in the myocardial area that corresponds to the control area of arteries, such as right coronary artery (RCA), left circumflex (LCX), left anterior descending (LAD). Each control area of arteries is divided into territories (see Fig.5).

The doctor specifies the injured coronary artery territories and its control area (as shown in Table 2). This is the key point for CAD labeling. For example, if the result is “There is a small defect in the lateroanterior wall due to ischemia in the perfusion area of LCx”, the patient is labeled CAD. If the result is “The result is properly normal”, the patient is labeled non-CAD. We developed a software for labeling the CAD (see Fig.6).

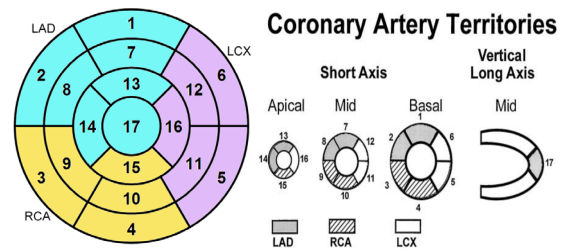


Fig. 5. A slice view of coronary artery territories as suggested by the American Heart Association.

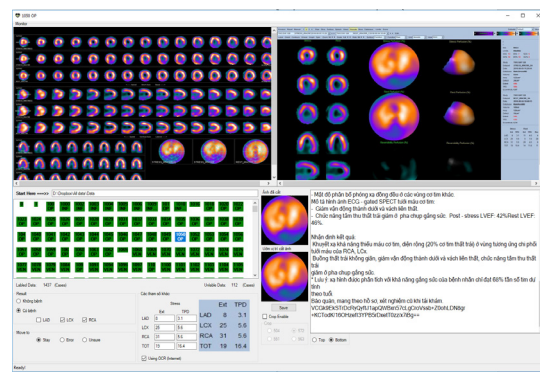


Fig. 6. The software used for labeling CAD/non-CAD patients.

Table 2. 17 coronary artery territories used in CAD diagnosis results.

| LAD | RCA | LCX |
|-----------------------|-----------------------|------------------------|
| 1. Basal anterior | 3. Basal inferoseptal | 5. Basal inferolateral |
| 2. Basal anteroseptal | 4. Basal inferior | 6. Basal anterolateral |
| 7. Mid anterior | 9. Mid inferoseptal | 11. Mid inferolateral |
| 8. Mid anteroseptal | 10. Mid inferior | 12. Mid anterolateral |
| 13. Apical anterior | 15. Apical inferior | 16. Apical lateral |
| 14. Apical septal | | |
| 17. Apex | | |

2.2. Diagnosis model

We develop our deep learning network based on the VGG network, which consists of 16 convolutional (CNN) layers and it is very appealing because of its very uniform architecture [14]. Our network includes 8 CNN layers, filter size of 3×3. Each CNN layer is followed by a BatchNormalization layer for normalizing data, then a Rectified Linear Unit (ReLU) activation function and a MaxPooling layer with stride 2. These CNN layers are used for extracting main features of input images. The output of CNN layers is passed through a GlobalAverage Pool to generate the feature vector. The fully connected (FC) layer with the softmax function is added to the end of the network. The last FC layer consists of 2 units (representing the CAD and non-CAD classes). Overview of our network is shown in Fig. 7.

The output of our proposed network is a 2-element vector $y = [p_{CAD}, p_{non-CAD}]$, in which each element represents the probability of classes: p_{CAD}

indicates the probability of CAD, $p_{non-CAD}$ indicates the probability of non-CAD, where $p_{CAD} + p_{non-CAD} = 1$. The output label of the network is assigned to the class with higher probability.

In our method, the slice MPI image is fed into the network for diagnosing the CAD. We also prove the efficiency of using the MPI image in CAD diagnosis compared to the polar map images. This is done by feeding the polar map image into the same network architecture. We assess the precision of our model by using k -fold cross validation, with $k = 5$. More precisely, our dataset is separated randomly into 5 equal subsets. Each subset consists of 282 (the last one has 285) images with average 154 (± 7) CAD and 128 (± 8) non-CAD. Four subsets were used for training and the other subset was used for testing. We repeated the training and testing procedure, each with different testing subset (see Fig. 8). The precision of the tested subset in each procedure was computed and recorded. The precision is the mean of the 5 recorded values.

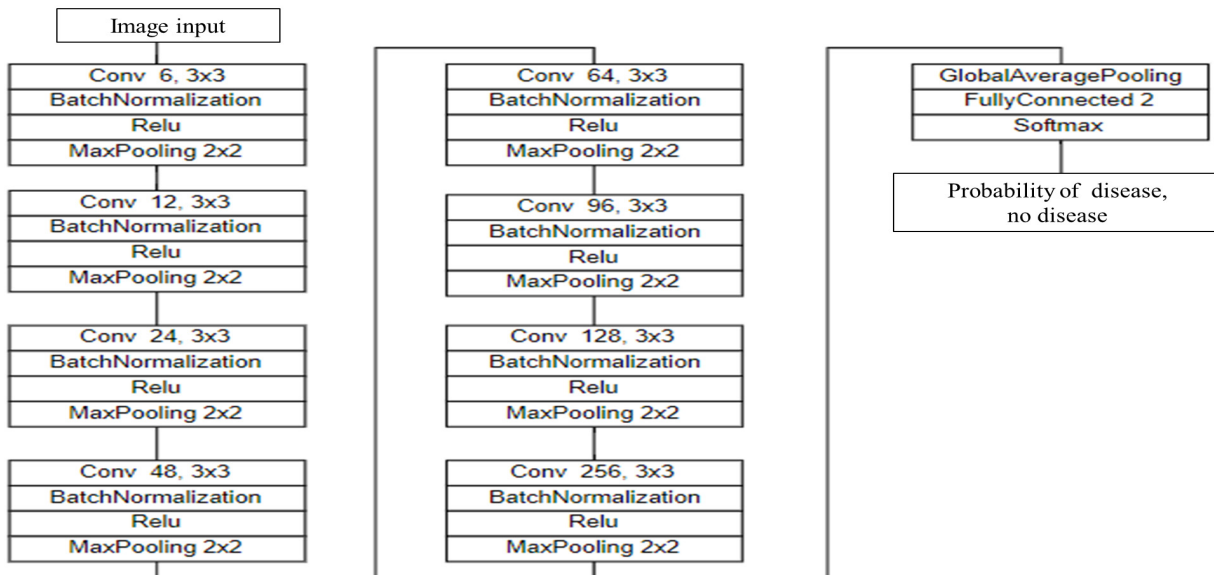


Fig. 7. Our deep learning network architecture used for diagnosing CAD.



Fig. 8. An illustration of 5-fold cross validation.

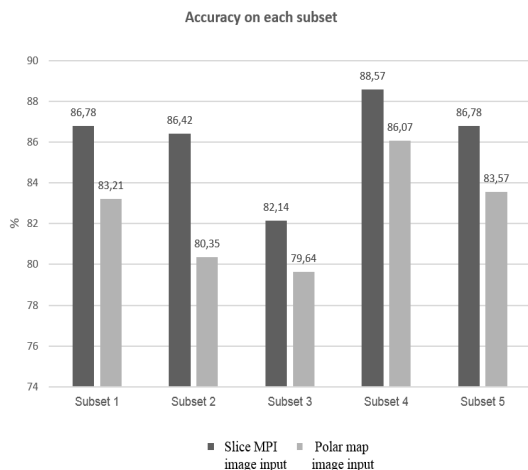


Fig. 9. Precision of two models using slice MPI images and polar map images on each subset

Our network model was built in Python with Keras API. The network was trained on a computer with configuration CPU Intel CoreI i3-6100 @ 3.70GHz; RAM: 8Gb; GPU: Nvidia GeForce GTX 1060 3GB.

The training time of the network with four subsets is about 1 hour and 13 minutes. The time for recognizing an image is about 50 milli seconds.

3. Experimental results and discussion

Experimental results indicate that deep learning model training with slice MPI produces higher diagnosis accuracy on all subset than using polar map (Figure 9). Figure 10 shows the mean precision of our proposed deep learning network using slice MPI images (86.14% ± 2.14%) and polar map images (82.57% ± 2.33%).

In additions, we also analyze the receiver operating characteristic (ROC) that illustrates the diagnostic ability. Fig.11 shows the ROC of the trained model using slice MPI and polar map images. The

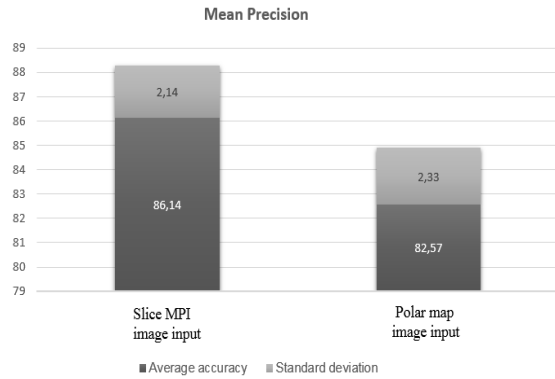


Fig. 10. Mean precision of two models using slice MPI images and polar map images.

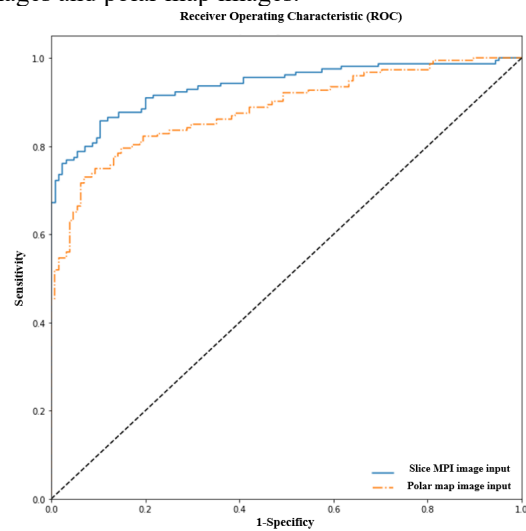


Fig. 11. ROC of the trained model using slice MPI and polar map images.

ROC curve of the model using slice MPI images is higher than that of model using polar map images. This indicates that model using slice MPI images has a higher diagnostic ability than model using polar map images.

4. Conclusion

This paper introduced a deep learning method for diagnosing the CAD using the slice images acquired from the SPECT camera. The performance of our method is better than the existing method.

With the same deep network, learning from slice images provides a higher accuracy of detecting CAD than from polar images. This is reasonable since polar images are synthesized from slices images and the synthesization probably does not maintain all the features of slice images. The experimental results suggest that slice images are helpful and should be used in diagnosing the CAD.

This study shows the potentiality of using SPECT slice images in diagnosing CAD by deep learning

methods. However, there is still space for improving the accuracy of detecting CAD. Our future work is to improve the performance of the CAD detection, such as polishing the image processing procedure since the input of the network in our experiment is not refined; and adding more information of patient, e.g. TPD parameters, age, gender, and past medical history.

References

- [1] Goff D. C., Jr., et al, 2013 ACC/AHA guideline on the assessment of cardiovascular risk: a report of the American College of Cardiology, American Heart Association Task Force on Practice Guidelines, *Circulation*, 129, 25 Suppl 2 (2014), 49-73.
- [2] Einstein AJ, Effects of radiation exposure from cardiac imaging: how good are the data?, *J Am Coll Cardiol* 59 (2012), 553–565.
- [3] Hongkai Wang, Zongwei Zhou, Comparison of machine learning methods for classifying mediastinal lymph node metastasis of non-small cell lung cancer from 18F-FDG PET/CT images, *EJNMMI Research* (2017), 7(1):11 .
- [4] Ryo Nakazato, Balaji K. Tamarappoo, Xingping Kang, Arik Wolak, Faith Kite1, Sean W. Hayes, Louise E.J. Thomson, John D. Friedman, Daniel S. Berman and Piotr J. Slomka, Quantitative Upright–Supine High-Speed SPECT Myocardial Perfusion Imaging for Detection of Coronary Artery Disease: Correlation with Invasive Coronary Angiography, *Journal of Nuclear Medicine* (2010), 51(11): 1724–1731.
- [5] Yann LeCun, Yoshua Bengio & Geoffrey Hinton, Deep learning, *Nature* (2015), 521, 436–444.
- [6] Varun Gulshan, PhD; Lily Peng, MD, PhD; Marc Coram, PhD; et al, Development and Validation of a Deep Learning Algorithm for Detection of Diabetic Retinopathy in Retinal Fundus Photographs, *JAMA*, (2016), 316(22).
- [7] Betancur, Commandeur, Motlagh, Deep Learning for Prediction of Obstructive Disease from Fast Myocardial Perfusion SPECT, *JACC: Cardiovascular Imaging* (2018), 11(11):1654-1663.
- [8] Peter L. Tilkemeier, MD, Standardized reporting of radionuclide myocardial perfusion and function, *Journal of Nuclear Cardiology* (2009).
- [9] Bateman TM, Dilsizian V, Beanlands RS, DePuey EG, Heller GV, Wolinsky DA, American society of nuclear cardiology position statement, *Journal of Nuclear Cardiology* (2016).
- [10] Matthew D. Zeiler and Rob Fergus, Visualizing and Understanding Convolutional Networks, *ECCV 2014: Computer Vision – ECCV (2014)*, 818-833.
- [11] Hesse B, et al, EANM/ESC procedural guidelines for myocardial perfusion imaging in nuclear cardiology, *European journal of nuclear medicine and molecular imaging*, 32(7) (2005), 855-897.
- [12] Holly T. A., et al, Single photon-emission computed tomography, *J Nucl Cardiol*, 17(5) (2010.), 941-973.
- [13] Available at [Http://www3.gehealthcare.ca/en/products/categories/nuclear_medicine/xeleris_workstations_and_applications/evolutionforcardiac](http://www3.gehealthcare.ca/en/products/categories/nuclear_medicine/xeleris_workstations_and_applications/evolutionforcardiac).
- [14] Karen Simonyan, Andrew Zisserman, Very Deep Convolutional Networks for Large-Scale Image Recognition, *ICLR* (2015).